Journal of Solid State Chemistry 294 (2021) 121857

Contents lists available at ScienceDirect

Journal of Solid State Chemistry

journal homepage: www.elsevier.com/locate/jssc

Fabricating iron-cobalt layered double hydroxide derived from metal-organic framework for the activation of peroxymonosulfate towards tetracycline degradation

Yue Wang [a,1], Jiao Cao [a,1], Zhaohui Yang [a,*], Weiping Xiong [a,d,**], Zhengyong Xu [b], Peipei Song [c], Meiying Jia [a], Saiwu Sun [a,d], Yanru Zhang [a], Wei Li [e]

[a] College of Environmental Science and Engineering, Hunan University and Key Laboratory of Environmental Biology and Pollution Control, Ministry of Education, Hunan University, Changsha, 410082, PR China
[b] Science and Technology Service Center of Hunan Province, Changsha, 410128, PR China
[c] College of Resources and Environment, Key Laboratory of Agricultural Environment, Shandong Agricultural University, Tai'an, 271000, PR China
[d] Hunan Dalu Technol Co Ltd, 559 Yunxi Rd, Changsha, 410036, Hunan, PR China
[e] Hunan Xinheng Environmental Technology Co Ltd, Changsha, 410005, PR China

ARTICLE INFO

Keywords:
FeCo-LDH
ZIF-67
Etch
PMS activation
Tetracycline

ABSTRACT

Herein, iron-cobalt layered double hydroxide (FeCo-LDH) was synthesized by sacrificing Co-containing zeolite imidazolate framework materials (ZIF-67) in iron ethanolic solution at room temperature. The catalytic performances of catalysts were investigated by activating peroxymonosulfate (PMS) for tetracycline (TC) degradation. Experimental results were demonstrated that FeCo-LDH with molar ratios of Fe and Co was 1.5 (FeCo-LDH-1.5) exhibited the highest catalytic activity, in which the TC degradation efficiency was reached to 92% within 5 min. The system of FeCo-LDH-1.5/PMS exhibited high stability and high efficiency in the influencing factor experiments including TC concentrations, initial pH, coexisting anions (Na^+, Cl^-, SO_4^{2-}) and humic acid (HA). Results of quenching experiments and electron paramagnetic resonance (EPR) characterization showed that $O_2^{\bullet-}$ and $SO_4^{\bullet-}$ radicals were the foremost reactive species for TC degradation. Liquid chromatograph - mass spectrometer (LC-MS) and three-dimensional excitation emission matrix fluorescence spectro photometer (3D EEMs) were conducted to investigate the degradation intermediate and possible degradation pathway. Moreover, high degradation efficiency was implemented in actual wastewater by the FeCo-LDH-1.5/PMS system. Compared to Fe^{3+}/PMS and Co^{2+}/PMS homogeneous system, the FeCo-LDH-1.5/PMS system was exhibited advantages in catalytic activity and high reusability. This study provided a convenient method to synthesis advanced hydrotalcite-like catalysts, which showed remarkable performance in actual wastewater treatment.

1. Introduction

Antibiotics are widely used as chemotherapeutic agents for the infectious disease therapy in humans, animals and plants because of sufficiently non-toxicity to the host [1]. According to the report, the consumption and production of antibiotics are increasing with the development of aquaculture and agriculture in China [2]. Due to overuse or abuse of antibiotics, the antibiotics can be detected in water environment and the concentration even up to few tens of ppb [3,4]. The concentration of antibiotics in soil and sediment increases with the occurrence of pollution, which induces the production of resistance genes [5] with potential toxic effect on humans and animals [6–11].

Nowadays, advanced oxidation processes (AOPs) have become the focus in environmental applications [12–14]. The AOPs can significantly oxidize and remove organic contaminants from wastewater without the production of second pollution [15–19]. As the practical application of $OH^{\bullet}$ - based Fenton system is always limited by low hydrogen peroxide utilization and strict pH requirements [20], peroxymonosulfate (PMS) - based AOPs with the generation of $SO_4^{\bullet-}$ radical exhibit advantages in the degradation of refractory organics [21]. Compared with the standard

* Corresponding author. College of Environmental Science and Engineering, Hunan University, Changsha, Hunan, 410082, China.
** Corresponding author. College of Environmental Science and Engineering, Hunan University, Changsha, Hunan, 410082, China.
E-mail addresses: yzh@hnu.edu.cn (Z. Yang), xiongweiping@hnu.edu.cn (W. Xiong).
[1] These authors contribute equally to this article.

https://doi.org/10.1016/j.jssc.2020.121857
Received 23 September 2020; Received in revised form 6 November 2020; Accepted 10 November 2020
Available online 12 November 2020

reduction potential of $OH^{\bullet-}$ (1.8–2.7 eV), $SO_4^{\bullet-}$ (2.5–3.1 eV) is higher under neutral environment [22], broader pH value from 2 to 9 [23] and remarkable selectivity for aromatic structure organics and unsaturated bonds [24,25]. Above all make $SO_4^{\bullet-}$ exhibit outstanding performance on degradation refractory organics. Transition metals including Cu, Fe, Co and Mn can activate PMS to generate $SO_4^{\bullet-}$ [26]. By contrast, cobalt ions (Co^{2+}) are the better effective mediator to activate PMS because of high catalytic efficiency and low dosage [27]. For instance, Li et al. synthesized FexCoy@C nanocages to activate PMS for the degradation of bisphenol A (BPA), the synergistic effect of iron and cobalt made the catalytic reaction more efficient [28].

Layered double hydroxides (LDHs) are assembled with metal hydroxide layer board and compensating anions in the interlayer region. These materials can be expressed as follows: $[M(II)_{1-x}M(III)_x(OH)_2]^{x+}[A^{n-}_{x/n}]^{x-}\blacksquare\, mH_2O$. M(II) and M(III) represent divalent and trivalent cations, respectively, A^{n-} represents interlayer anion and x is generally in the range of 0.2–0.4 [29]. Conventional synthetic methods of LDHs including co-precipitation, hydrothermal and ion-exchange, which not only require strict experimental conditions but also obtain heterogeneous component [30–33]. Zhang et al. synthesized $NiFe_2O_4$/ZnCuCr-LDH had strict requirements on the pH of the reaction system, and required high-temperature reactions in reaction kettles [34]. Compared with the severe operating conditions of traditional methods, the template sacrifice method in this study can be completed in mild conditions. Metal-organic framework materials (MOFs) are composed of clusters or metal ions and organic ligands by coordination mode, which exhibit one- or more-dimensional structures [35–39]. MOFs with large specific surfaces and high porosity are researched in the catalytic reaction, adsorption, gas storage and sensing fields [40–44]. MOFs also have been investigated as active elements in energy-related devices, owing to their outstanding features [45–48]. As a typical category of MOFs, Co-containing zeolite imidazolate framework materials (ZIF-67) with uniform distribution of Co atoms and vibrant pores seemed to be an excellent precursor to fabricate LDH homogeneously [49]. The exposed Co sites can be hydrolyzed and precipitated to generate LDHs [50]. In the etching process, other metal ions can partially replace the Co ions in ZIF-67 and enhance its performance. Jiang et al. synthesized Ni–Co LDH nanocages with templates of ZIF-67, the novel hierarchical and submicroscopic structures brought superior pseudocapacitance property [51]. Cao et al. synthesized AlCo-LDH with templates of Co-ZIF, which was exhibited high efficiency to PMS activation [12].

Herein, a convenient synthesis of iron-cobalt layered doubled hydroxides (FeCo-LDH) by sacrificing ZIF-67 templates was provided. The formation process of FeCo-LDH was demonstrated in detail, and the tetracycline (TC) was selected as the objective pollutant for measuring catalytic activity of samples. The synthesized FeCo-LDH with the heterogeneous feature promoted the PMS activation for TC removal. The morphology, composition, structure and textural properties of FeCo-LDH catalysts were tested by corresponding characterization tests. To highlight the advantages of heterogeneous FeCo-LDH catalyst, the comparative experiment of homogeneous and heterogeneous catalytic performance and cycle experiments were carried out. Simultaneously, the effects of TC concentrations, initial pH, co-existing ions, water bodies were considered. Degradation mechanism of FeCo-LDH/PMS system towards TC based on the tripping experiments, EPR characterization and electrochemical characterizations was discussed in-depth. This research was mainly introduced a newly, efficient and valuable method to design MOF-derived catalyst for actual sewage treatment.

2. Experimental section

2.1. Chemical agents

Cobalt nitrate hexahydrate ($Co(NO_3)_2{\cdot}6H_2O$, ≥99.9%), Ferric nitrate hydrate ($Fe(NO_3)_3{\cdot}9H_2O$, ≥97%), 2-methylimidazole (H-mim, ≥99%), methanol (≥99.5%) and ethanol (≥99.9%) were purchased from the Sinopharm Chemical Reagent Co. Ltd. Shanghai Rhawn Technology Development Co. Ltd provided potassium peroxymonosulfate (PMS, 42%–47% $KHSO_5$ basis) and tetracycline (99%). All solutions in experiments were prepared in the water which purified by the Milli-Q system (resistivity > 18 MΩ cm).

2.2. Materials preparation

Synthesis of ZIF-67: 5 mmol $Co(NO_3)_2{\cdot}6H_2O$ and 20 mmol 2-methylimidazole were dissolved in methanol (50 mL), respectively. Then, the solution contained 2-methylimidazole was slowly added into $Co(NO_3)_2{\cdot}6H_2O$ solution and stirred the mixed solution for 24 h. Then, the products were collected and washed with methanol for several times. In the end, products were dried in vacuum at 60 °C to obtain ZIF-67.

Synthesis of FeCo-LDH: 0.5 g ZIF-67 was mixed in 40 mL ethanol containing $Fe(NO_3)_3{\cdot}9H_2O$ (0.5 mmol–2 mmol) under stirring for 1 h respectively. The collected samples were washed with ethanol and dried in vacuum at 60 °C to obtain FeCo-LDH.

2.3. Experiments method

Two steps conducted the experiments of TC removal. Firstly, 20 mg of samples were added into the 100 mL of 30 mg L^{-1} TC solution with continuously magnetic stirring for 60 min. Then, 25 mg of PMS was added into the above mixed solution and stirred for 30 min. The pH value of TC solution was unadjusted in the experiment unless the specified experiment. All experiments were repeated at least three times, and the error bar was shown in the figures.

3. Results and discussion

3.1. Structure characterization

As shown in the scanning electron microscopy (SEM) figures, the pristine ZIF-67 was exhibited a homogeneous rhombic dodecahedron morphology with smooth surface, which were useful for preparation of porous MOFs derivatives by in-situ etching process (Fig. 1a). The as-obtained ZIF-67 showed high purity and crystallinity, and the XRD pattern was same as the simulated pattern (Fig. 2a). After in-situ etching in 0.5 mM iron ethanol solution, the surface of the as-obtained FeCo-LDH-0.5 became rough, and the particle morphology was similar with the pristine ZIF-67 (Fig. 1b). Obviously, when the ZIF-67 particles were etched in 1.5 mM iron ethanol solution, the morphology of the obtained FeCo-LDH-1.5 was quite different, a huge hierarchical structure. (Fig. 1c). In XRD pattern of as-prepared FeCo-LDH samples (Fig. 2b), the crystallinity of FeCo-LDH-1.5 decreased and the characteristic peaks were matched well with (003), (006) and (012) facets of the reported FeCo-LDH, suggesting the synthesized sample was mainly consisted of FeCo-LDH [52].

Elemental mapping based on SEM mode was displayed the compositional distribution of FeCo-LDH. As showed in Fig. 1 (d)~(o), the content of O and Fe elements were increased and the content of Co element was decreased with the increase of the ratio of Fe and Co elements. In the ultimate FeCo-LDH-1.5, the O, Co and Fe elements were uniformly distributed. From the above characterizations, the formation of FeCo-LDH was hypothesized as followed. The dissolution of ZIF-67 template and reconstruction of FeCo-LDH were occurred synchronously in the etching process. In the pores of ZIF-67, excessive amount of water molecules coordinated with the cobalt ions. When used iron ethanolic solution as the etchant, the numerous ethanol was replaced the H_2O and released iron ions. The released Fe^{3+} ions in solution were hydrolyzed ($Fe^{3+} + 3H_2O$–$Fe(OH)_3 + 3H^+$). The generated H^+ protons were etched the ZIF-67 ($Co(N–N)_2 + 2H^+$ —— $Co^{2+} + 2(N–NH)$) and freed Co^{2+} ions were hydrolyzed as well ($Co^{2+} + 2H_2O$–$2Co(OH)_2 + 2H^+$) [53]. The pH value of the solution after etching procession was 5.49 ± 0.4, confirming the above hydrolytic process. While the pH value of initial iron ethanolic

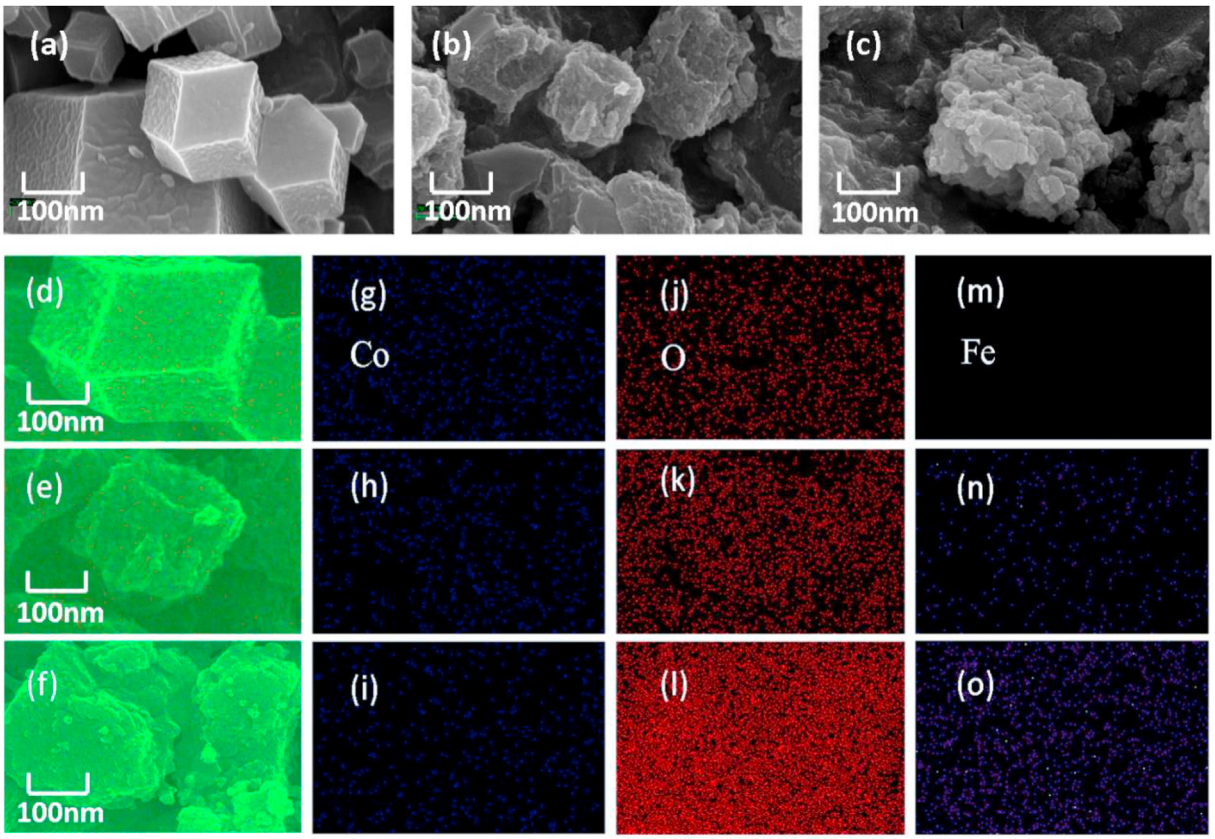

Fig. 1. SEM images of ZIF-67 (a), FeCo-LDH-0.5 (b) and FeCo-LDH-1.5 (c) samples in the 100 nm magnification. EDS mappings of the selected protion in ZIF-67 (d), FeCo-LDH-0.5 (e) and FeCo-LDH-1.5 (f) samples: difference of Co (g ~ i), O (j ~ l) and Fe (m ~ o).

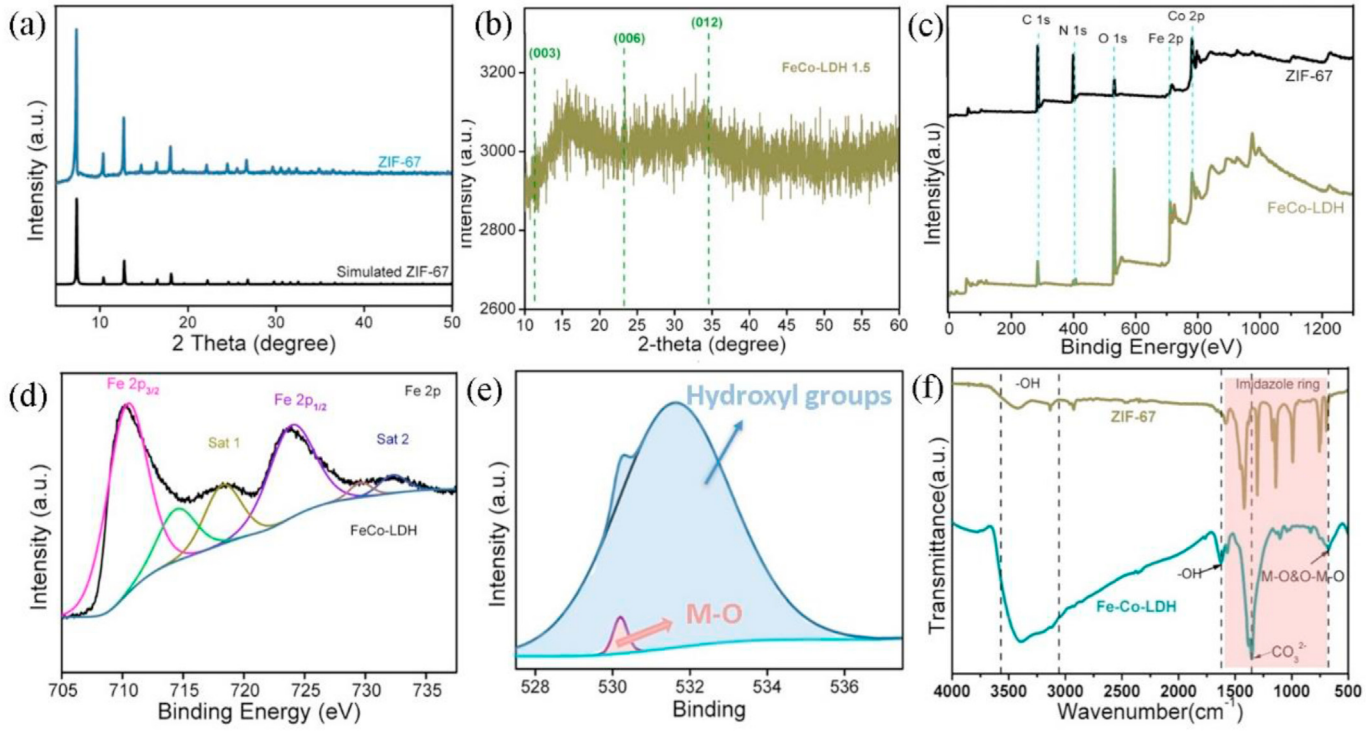

Fig. 2. XRD patterns of ZIF-67 (a) and FeCo-LDH-1.5 (b); XPS analysis of survey spectrums of ZIF-67 and FeCo-LDH-1.5 (c), Fe 2p spectrum of FeCo-LDH-1.5 (d) and O 1s spectrum of FeCo-LDH-1.5 (e); FT-IR spectra of ZIF-67 and FeCo-LDH-1.5 (f).

solution was almost unmeasured, suggesting the quite low content of H^+ protons [12]. The slightly acidic condition was contributed to the deconstruction process. Based on the uniform composition of organic linkers and metal centers in ZIF-67, the etching process occurred evenly in the whole structure. Therefore, all elements were uniformly distributed in the obtained samples, which were well matched to the EDS mapping results. Finally, numerous H^+ protons were leaded to the hydrolysis equilibrium. Furthermore, ethanol as the solvent was conductive to retard the etching process of ZIF-67 and prevented impurity [51].

From the typical X-ray photoelectron spectroscopy (XPS) survey spectrum in Fig. 2c, the C 1s, O 1s, N 1s and Co 2p peaks were occurred in ZIF-67 spectrum, while only O 1s and Fe 2p peaks were remarkable appeared in the FeCo-LDH-1.5 spectrum. Moreover, the Fe and Co content in FeCo-LDH-1.5 were 21.16% and 11.61%, respectively, these results were occurred in ICP-MS test and closed to the XPS analysis. Above results suggested the incorporative Fe^{3+} was replaced Co^{2+} to synthesize hydrotalcite-like FeCo-LDH. Fig. 2e exhibited O 1s spectra of FeCo-LDH-1.5, there was a strong peak at 531.50 eV belonged to the hydroxy species, suggesting the existence of abundant hydroxyl groups in FeCo-LDH-1.5, and the meaning of the pink area in the O 1s spectrum is the characteristic peak of M − O, this signal was confirmed the existence of the vibrations mode of metal-oxygen (M − O) [54]. As shown in Fe 2p spectrum (Fig. 2d), the fitting peaks at 710.35 eV and 723.90 eV were belonged to Fe 2p3/2 and Fe 2p1/2, respectively. Two satellite peaks located at 716.90 eV and 732.25 eV were indicated the presence of Fe^{3+} [52,55]. The existence of the peak at 713.55 eV was implied that the Fe^{3+} species were presented in more coordination environment, which caused by the high affinity of neighbouring Co^{2+} ions [56]. Two main peaks represented Co 2p3/2 and Co 2p1/2 were occurred in the spectrum of Co 2p (Fig. S1), and the existence of two satellite bands located at 785.95 eV and 795.50 eV was indicated that the Co ion in the FeCo-LDH-1.5 was in a high-spin Co^{2+} state [57].

From FT-IR test results (Fig. 2f), the characteristic peaks existed in the broad range of 3427–3503 cm^{-1} and 1630 cm^{-1}, which were ascribed to the hydroxyl groups stretching vibration. Different with the ZIF-67, the FeCo-LDH-1.5 exhibited a quite strong absorption on above area, indicating a successful formation of metal hydroxide and confirming the hypothesis about O 1s spectrum in XPS result. Meanwhile, a strong absorption peak at 1356 cm^{-1} was corresponded to CO_3^{2-}, suggesting that inorganic anions were existed in interlayer [58]. The pink characteristic peaks occurred in the range of 700–1600 cm^{-1} was associated to the 2-methylimidazole ligand. In this range, all peaks were weak for FeCo-LDH, suggesting the removal of organic linkers from ZIF-67 [59]. The peak at 678 cm^{-1} represented the vibrations mode of metal-oxygen (M − O) or metal-hydroxyl (M − OH) group (M = Fe & Co) was observed in the spectra of FeCo-LDH-1.5, which was well matched to the O 1s and Fe 2p spectrum in XPS result. Above results were confirmed the layered double hydroxides structure of FeCo-LDH with interlayer exchangeable CO_3^{2-} anions.

As shown in Table S1, the BET pore diameter of FeCo-LDH-1.5 was 3.697 nm, which was closed to the pore diameter of ZIF-67, indicating that FeCo-LDH-1.5 was inherited the pore structure from the pristine ZIF-67. However, the decrease of surface area of FeCo-LDH-1.5 probably was caused by the high iron concentration, which made ZIF-67 dissolve rapidly and the ZIF-67 skeleton collapsed [51]. From the image of N_2 adsorption-desorption isotherms inserted with pore size distributions of samples (Fig. S2), the N_2 adsorption-desorption isotherms of ZIF-67 and FeCo-LDH-1.5 were type I hysteresis loops, as defined by International Union of Pure and Applied Chemistry (IUPAC), suggesting that there were a large number of micropores in the samples. Furthermore, the pore sizes were distributed in 0–5 nm.

3.2. Catalytic performance

The catalytic properties of samples were evaluated by PMS activation for the TC removal. In the system of only PMS and ZIF-67/PMS, the removal efficiency of TC was 48% and 39%, respectively. Obviously, in the FeCo-LDH-0.5/PMS, FeCo-LDH-1/PMS, FeCo-LDH-1.5/PMS and FeCo-LDH-2/PMS system, the TC removal efficiency were reached up to 62%, 73%, 92% and 94%, respectively. Consideration of saving costs and high catalytic performance, the FeCo-LDH-1.5 would be better than others (Fig. 3a). In addition, the humic acid with concentrations of 0–9 mg L^{-1} was exhibited a minor inhibition on TC oxidation (Fig. 3d). Likewise, a weak impacted on the TC removal also occurred in the existence of inorganic species (e.g. Cl^-, SO_4^{2-} and Na^+) with different concentrations (Fig. 3b∼3c). These results suggested that FeCo-LDH-1.5/PMS system could suffer small obstruction from usual background inorganic and organic substance in water.

3.3. Catalytic mechanism

The quenching tests were conducted to study the TC degradation mechanism and the involvement of radicals. As reported, phenol was used to capture all active substance. Methanol was a capture agent for sulphate radical ($SO_4^{\bullet-}$) and hydroxyl radical ($OH^{\bullet}$). Tertiary butanol (TBA) was used for quenching $OH^{\bullet}$ radical. P-benzoquinone was added to capture the radical of superoxide ($O_2^{\bullet-}$) [60]. As presented in Fig. 4a, the degradation efficiency was dramatically declined to 46% with the addition of phenol, indicating that the degradation of TC in the system of FeCo-LDH-1.5/PMS was mainly depended on the role of active substance. When added methanol and TBA, TC degradation efficiency was reduced from 92% to 72% and 88%, respectively. Thus, $SO_4^{\bullet-}$ and $OH^{\bullet}$ radicals were responsible for the observed removal efficiency. $OH^{\bullet}$ had nearly similar rate constants ($k_{methanol} = 9.7 \times 10^8\ M^{-1}\ s^{-1}$ and $k_{tertiary\ butanol} = 3.3 \times 10^9\ M^{-1}\ s^{-1}$), when reacted with methanol and TBA. While $SO_4^{\bullet-}$ was significantly high reactive to methanol ($1.0 \times 10^7\ M^{-1}\ s^{-1}$) compared to TBA ($4.0 \times 10^5\ M^{-1}\ s^{-1}$) [61]. Therefore, the lower capture influence of TBA demonstrated that $SO_4^{\bullet-}$ was the dominant active species produced by the system of FeCo-LDH-1.5/PMS. Furthermore, the removal efficiency was declined to 56% with the addition of P-benzoquinone, which implied the critical role of $O_2^{\bullet-}$ radicals.

Above all, the $SO_4^{\bullet-}$ and $O_2^{\bullet-}$ radicals were acted as the dominant radicals in the TC degradation process. The electron paramagnetic resonance (EPR) technology was carried out to confirm the above quenching tests. After added 5,5-dimethyl-pyrroline-oxide (DMPO), the characteristic peaks of DMPO- $SO_4^{\bullet-}$ were clearly observed in the system of FeCo-LDH-1.5/PMS after 10 min compared to the weak peaks in PMS solution (Fig. 4b). Moreover, a series of characteristic signals were found in Fig. 4c by dropping into 2,2,6,6 -tetramethyl-4-piperidinyl (TMP), suggesting the existence of $O_2^{\bullet-}$ radicals. All these characterization results were further proofed that $SO_4^{\bullet-}$ and $O_2^{\bullet-}$ radicals were acted as the dominant active species for the TC degradation.

As the FeCo-LDH-1.5 with unique hydrotalcite-like layered structure inherited the high porosity from ZIF-67 templates, TC molecules could react with the active sites more fully. In addition, the electronegativity (11.9 eV) of Co was higher than Fe (10.1 eV), which probably occurred a shift of electron cloud from Fe ions to Co ions [62–64]. Therefore, with the help of Fe ions, the electron-rich Co site could be better to activate PMS. To further verify the proposed electron transfer process, linear sweep voltammetry (LSV) experiments were conducted (Fig. S3). When working condition was bar FTO glass as working electrode in the electrolyte containing PMS and TC, there was no apparent current response. While the ZIF-67-FTO was selected as working electrode, there was a slight current increase in the same electrolyte. A significant current increase could be observed by changing working electrode to FeCo-LDH-1.5-FTO, confirming the prompt electron transfer in the system of TC, PMS and FeCo-LDH-1.5-FTO working electrode. Above results suggested the importance of all parts (FeCo-LDH-1.5 particles, PMS and TC) in the reaction system and supported the proposed ternary system.

Based on the XPS analysis, Co ions and Fe ions were existed in FeCo-LDH-1.5 with bivalent state and trivalent state, which could activate PMS (HSO_5^-) to generate powerful oxidizing species ($SO_4^{\bullet-}$ and $O_2^{\bullet-}$). Firstly,

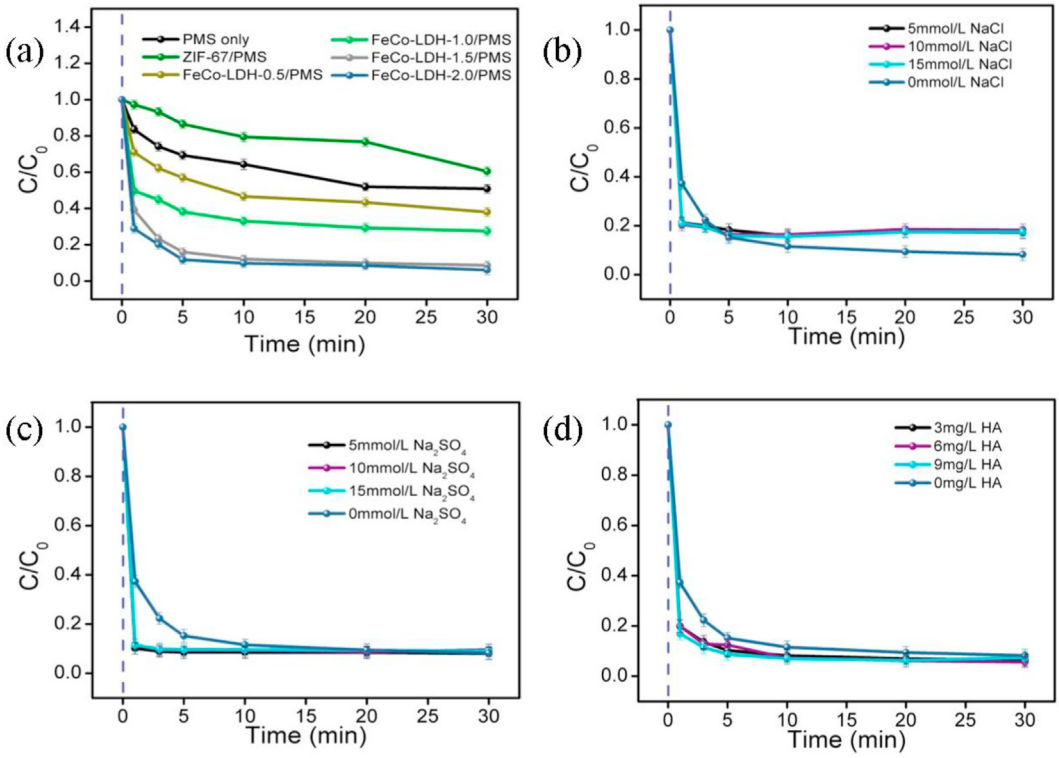

Fig. 3. Catalysis degradation of TC on different catalysts (a); Effects of NaCl (b); Na_2SO_4 (c) and humid acid (d). Experimental conditions: catalyst dosage = 0.2 g L^{-1}; initial TC concentration = 0.3 g L^{-1}; PMS concentration = 0.25 g L^{-1}

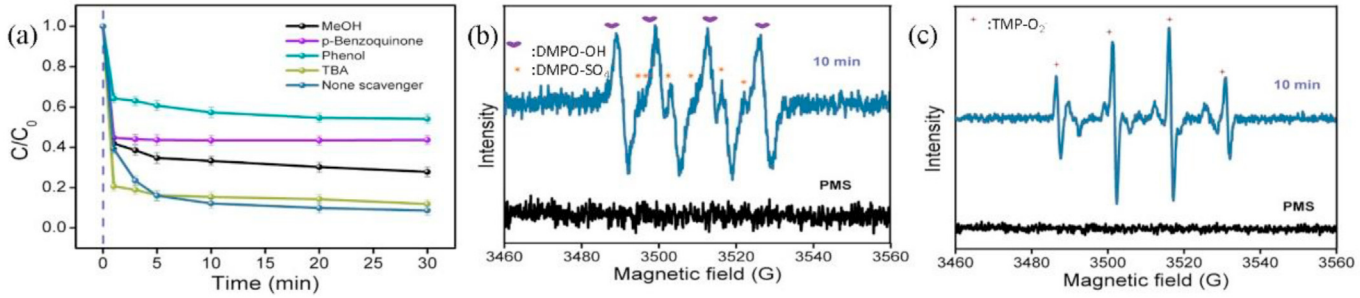

Fig. 4. Removal efficiency of FeCo-LDH-1.5/PMS system with different redical scavengers for TC degradation (a); EPR spectra for FeCo-LDH-1.5/PMS system in aqueous dispersion by spin trapping with DMPO (b) and TMP (c). Experimental conditions: catalyst dosage = 0.2 g L^{-1}; initial TC concentration = 0.3 g L^{-1}; PMS concentration = 0.25 g L^{-1}

Co^{2+} oxidized to Co^{3+}, and Fe^{3+} reduced to Fe^{2+} with the presence of HSO_5^-. Excessive Co^{3+} ions and Fe^{2+} ions generated and reacted with HSO_5^- again. Then Co^{2+} and Fe^{3+} regenerated [65–67]. The redox cycle of Fe^{3+}/Fe^{2+} and Co^{2+}/Co^{3+} could activate PMS for the generation of $SO_4^{\bullet-}$, which also improved the generation process of $O_2^{\bullet-}$ and realized efficient catalytic oxidation. The activation mechanism of PMS with the FeCo-LDH-1.5 was described by Eqs. (1)–(6). All these reactive radicals ($SO_4^{\bullet-}$ and $O_2^{\bullet-}$) could effectively degrade TC. The possible degradation mechanism of TC by FeCo-LDH-1.5/PMS system was exhibited in Fig. 5

$$Co^{2+} + HSO_5^- \rightarrow Co^{3+} + SO_4^{\cdot-} + OH^- \quad (1)$$

$$Co^{3+} + HSO_5^- \rightarrow Co^{2+} + SO_5^{\cdot-} + H^+ \quad (2)$$

$$Fe^{3+} + HSO_5^- \rightarrow Fe^{2+} + SO_5^{\cdot-} + H^+ \quad (3)$$

$$Fe^{2+} + HSO_5^- \rightarrow Fe^{3+} + SO_4^{\cdot-} + OH^- \quad (4)$$

$$HSO_5^- + H_2O \rightarrow HSO_4^- + H^+ + HO_2^{\cdot-} \quad (5)$$

$$HO_2^{\cdot-} \rightarrow H^+ + O_2^{\cdot-} \quad (6)$$

3.4. TC degradation pathway

The degradation process of TC was detected by 3D EEMs, which could reflect the mineralization ability of advanced oxidation catalyst to some extent. As shown in Fig. 6, none fluorescence signal exhibited in the original solution, which taken from the dark reaction adsorption for 60 min, suggesting that there was no degradation of TC in the adsorption reaction under dark condition. After added PMS for catalytic oxidation, one fluorescence peak located at the range of Ex/Em = (325–375 nm)/(475–550 nm) occurred, indicating the beginning of the TC degradation. This characteristic peak was represented the humic acids-like fluorescence region [68]. Besides, with the time of catalytic oxidation increased from 5 min to 10 min, the fluorescence signal was gradually increased

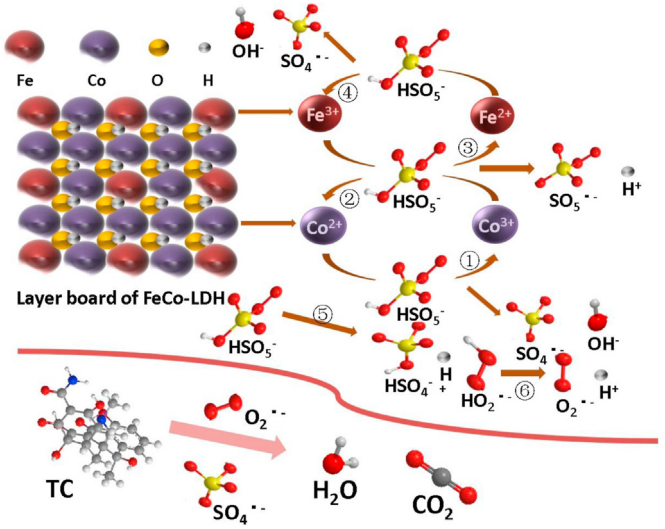

Fig. 5. Possible reaction mechanism of TC degradation by FeCo-LDH-1.5/PMS system.

and reached a maximum, demonstrating that TC was decomposed in-depth. When catalytic oxidation time achieved to 120 min, the fluorescence intensity was reduced obviously, and another fluorescence peak gathered at Ex/Em = (300–350 nm)/(375–450 nm) could be found, suggesting that humic acids-like matter was converted into CO_2 and H_2O. Moreover, there was a weak fluorescence peak at the range of Ex/Em = (325–375 nm)/(475–550 nm), which was confirmed the generation of other small molecules in the degradation process of humic acids-like matter. Liquid chromatograph - mass spectrometer (LC-MS) test was carried out to further discuss the TC degradation. These main mass peaks at m/z = 426, m/z = 409, m/z = 393, m/z = 363, m/z = 348, m/z = 283, m/z = 261, m/z = 247, m/z = 225 in the process of TC degradation were exhibited in Fig. 7a. From the figure of proposed transformation pathways of TC degradation (Fig. 7b), the TC molecules were attacked by the reactive radicals ($SO_4^{\bullet-}$ and $O_2^{\bullet-}$) and transformed to low molecular weight products via dealkylation, deamination, dehydration and ring - opening process [69], which was provided a more detailed degradation process. Therefore, TC was degraded into the humic acids-like matter at first and finally transferred to CO_2 and H_2O. Moreover, the TOC analysis was presented the 79.67% of TOC removal rate in the FeCo-LDH-1.5/PMS system. This result was suggested the existence of other small molecules in the system after complete degradation, which was matched well to the result of 3D EEMs test.

3.5. Effects of operating parameters on TC degradation and reusability

The operating parameters effects on the TC degradation were systematically evaluated to explore the oxidative character of the FeCo-LDH-1.5/PMS system. In the figure of the removal efficiency on different TC concentrations (Fig. 8a), when TC concentration was lowest as 5 mg L^{-1}, the removal rate was highest as 99.9%, which was closed to complete degradation. The content of TC in actual water was very low, which was suggested above result was of great significance. During the increase of TC concentration, the removal efficiency of TC was kept a high level under the same FeCo-LDH-1.5/PMS condition. These results were proved the remarkable degradation performance of TC in the FeCo-LDH-1.5/PMS system. From the figure of pH influence, the variation of pH value in the range of 3–9 was presented a negligible effect on the degradation of TC. At alkaline pH (pH = 11) environment, the degradation efficiency of TC was decreased, which was caused by the conversion from $SO_4^{\bullet-}$ to $HO^{\bullet-}$ under alkaline environment (Fig. 8b) [67]. This conversion was probably caused the consumption of the dominant $SO_4^{\bullet-}$ radical, which was the reason to the decrease of the degradation efficiency of TC. Even in the actual water environment such as tap water, river water and medical wastewater (The quality parameters of water bodies were presented in Table 1), the FeCo-LDH-1.5/PMS system was kept a high degradation efficiency of TC (Fig. 8c). While the slight decrease probably ascribed to the presence of organic matters in actual water, which could consume part of reactive radicals.

The degradation efficiency of FeCo-LDH-1.5/PMS was higher than the homogeneous catalysis system including Fe^{3+}/PMS and Co^{2+}/PMS (Fig. 8d). From a practical perspective, the reusability of the heterogeneous catalyst was significant for the decrease of operating costs. The

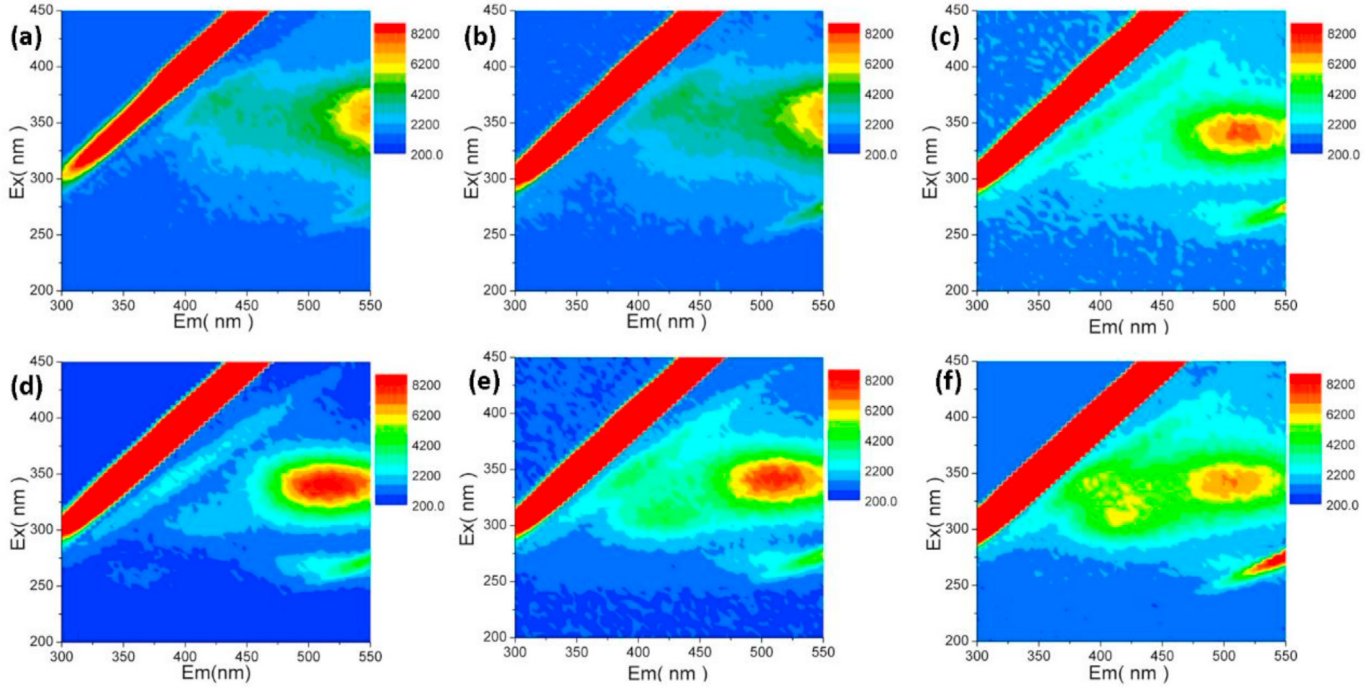

Fig. 6. The 3D EEMs analysis of TC intermediates in the degradation reaction of FeCo-LDH-1.5.

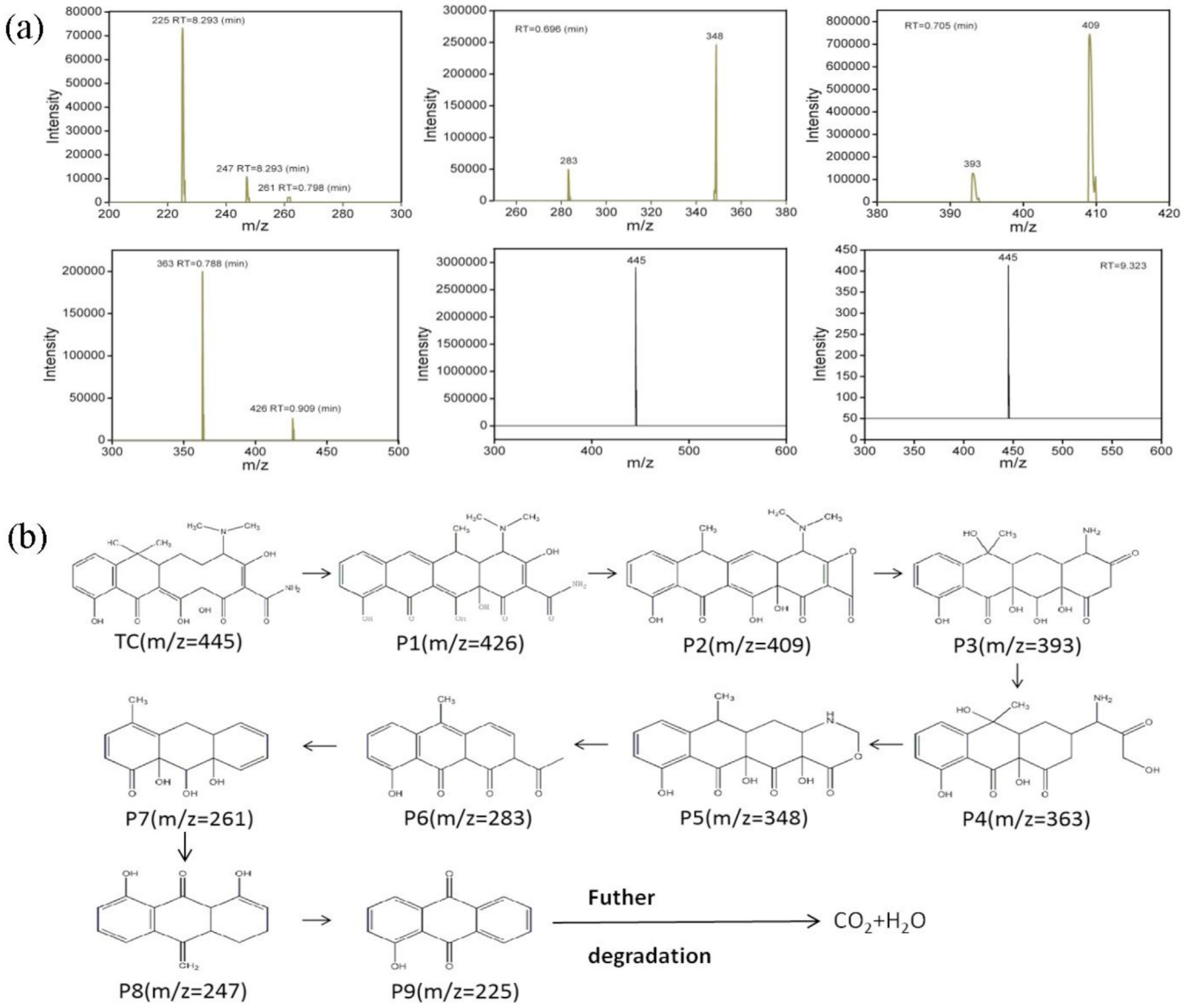

Fig. 7. LC-MS analysis of TC intermediates in the degradation reaction with FeCo-LDH-1.5.

cycle tests were conducted by repeatedly using FeCo-LDH-1.5/PMS as heterogeneous catalyst system for the degradation of TC under the identical conditions. As shown in Fig. S4, in the system of FeCo-LDH-1.5/PMS, the degradation efficiency was decreased to 84% after three cycles. From the results of ICP-MS test, the Fe and Co content in the initial FeCo-LDH were 21.16% and 11.61%, respectively. After three cycles, the Fe and Co content were changed to 23.49% and 8.85%, respectively. These results suggested that the Co element probably was leached from the FeCo-LDH-1.5 in the catalysis process, which might be caused the decrease of catalysis performance. Moreover, the difference of FT-IR spectrum of FeCo-LDH-1.5 before and after the three cycles experiments indicated the change of catalyst, which was no benefit to the catalysis process (Fig. S5).

4. Conclusion

In summary, FeCo-LDH-1.5 with thin nanoplatelets had been synthesized by in-situ etching ZIF-67 templates. The removal efficiency of TC under the FeCo-LDH-1.5/PMS system was reached up to 92%, which was much higher than ZIF-67/PMS system and Fe^{3+}/PMS, Co^{2+}/PMS homogeneous system. The FeCo-LDH inherited the high porosity from the ZIF-67 templates made TC molecules interact with reaction sites more completely. Moreover, Fe ions with lower electronegativity were helped Co ions to pass electrons to PMS efficiently. The $SO_4^{\bullet-}$ and $O_2^{\bullet-}$ radicals were acted as the major reactive species to the degradation of TC, which was proved by quenching tests and EPR analysis. Furthermore, 3D EEMs and LC-MS were applied to explore TC degradation pathway, which included dealkylation, deamination, dehydration and ring - opening process. 79.67% removal efficiency of TOC was directly confirmed the superiority of FeCo-LDH-1.5/PMS system. Effects of operating parameters including TC concentrations, the initial value of pH, normal background organic (HA) and inorganic armamentarium (Na^+, Cl^-, SO_4^{2-}) on the catalytic performance of FeCo-LDH-1.5 were exhibited excellent stability and practical value. Recycle tests were emphasized the reusability of FeCo-LDH-1.5. This work researched the combination of ZIFs and hydrotalcite by a simple method, which could have broad application of advanced oxidation.

CRediT authorship contribution statement

Yue Wang: Experimental operation, Data curation, and original draft preparation. **Jiao Cao:** Software, Validation. **Zhaohui Yang:**

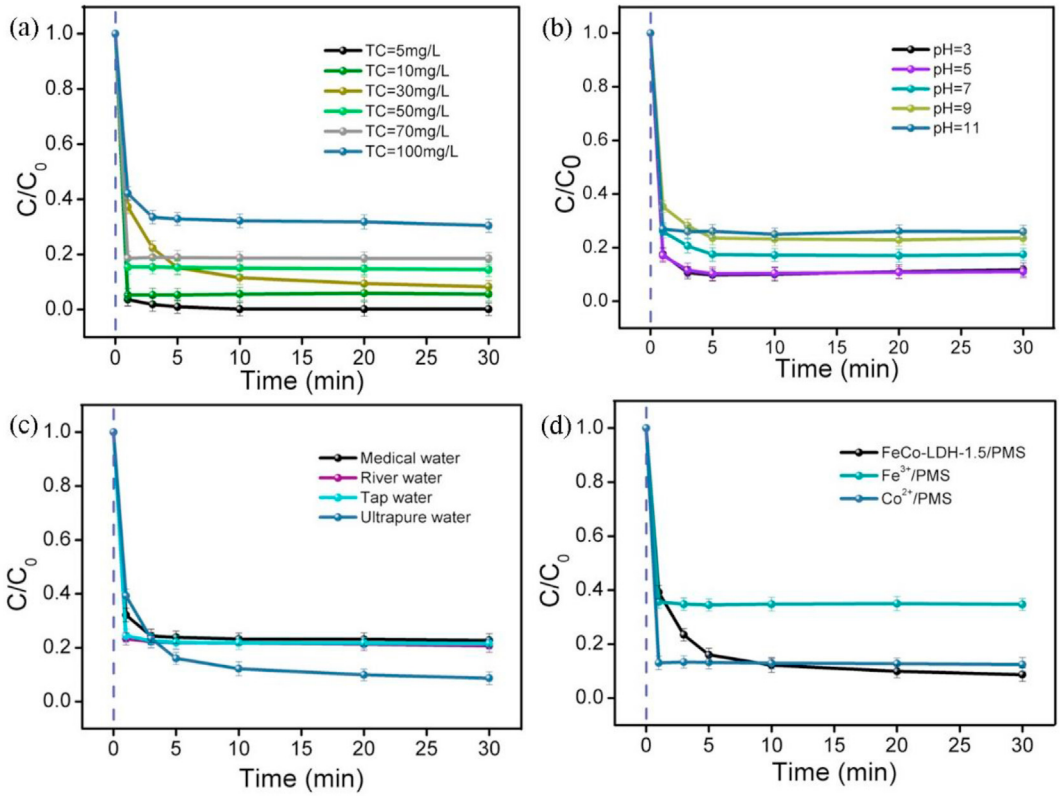

Fig. 8. Effects of TC concentration (a) and initial pH value (b) on TC degradation by FeCo-LDH-1.5; Removal efficiency of TC by FeCo-LDH-1.5 in real samples (c) and homogeneous catalysis system (d). Experimental conditions: catalyst dosage = 0.2 g L^{-1}; initial TC concentration = 0.3 g L^{-1}; PMS concentration = 0.25 g L^{-1}

Table 1
The quality parameters of tap water, river water and medical.

Water type	pH	COD (mg·L^{-1})	TOC (mg·L^{-1})
Tap water	7.50	1.843	0.721
River water	7.63	49.76	21.43
Medical water	6.62	25463	5148.22

Supervision. **Weiping Xiong:** Writing - review & editing. **Zhengyong Xu:** Investigation. **Peipei Song:** Writing - review & editing. **Meiying Jia:** Writing-reviewing. **Saiwu Sun:** Writing-reviewing. **Yanru Zhang:** Investigation. **Wei Li:** Investigation.

Declaration of competing interest

The authors declare that they have no known competing financial interests or personal relationships that could have appeared to influence the work reported in this paper.

Acknowledgements

This study financially supported by the National Natural Science Foundation of China (51878258 and 51521006 and 41807125).

Appendix A. Supplementary data

Supplementary data related to this article can be found at https://doi.org/10.1016/j.jssc.2020.121857.

References

[1] K. Kummerer, Antibiotics in the aquatic environment - a review - Part I, Chemosphere 75 (2009) 417–434.
[2] X.H. Liu, S.Y. Lu, W. Guo, B.D. Xi, W.L. Wang, Antibiotics in the aquatic environments: a review of lakes, China, Sci. Total Environ. 627 (2018) 1195–1208.
[3] X.H. Liu, Y. Liu, S.Y. Lu, X.C. Guo, H.B. Lu, P. Qin, B. Bi, Z.F. Wan, B.D. Xi, T.T. Zhang, S.S. Liu, Occurrence of typical antibiotics and source analysis based on PCA-MLR model in the East Dongting Lake, China, Ecotox, Environ. Safe. 163 (2018) 145–152.
[4] R. Xu, Z.-H. Yang, Y. Zheng, H.-B. Zhang, J.-B. Liu, W.-P. Xiong, Y.-R. Zhang, K. Ahmad, Depth-resolved microbial community analyses in the anaerobic co-digester of dewatered sewage sludge with food waste, Bioresour. Technol. 244 (2017) 824–835.
[5] Y. Bai, R. Xu, Q.-P. Wang, Y.-R. Zhang, Z.-H. Yang, Sludge anaerobic digestion with high concentrations of tetracyclines and sulfonamides: dynamics of microbial communities and change of antibiotic resistance genes, Bioresour. Technol. 276 (2019) 51–59.
[6] Y.G. Zhu, T.A. Johnson, J.Q. Su, M. Qiao, G.X. Guo, R.D. Stedtfeld, S.A. Hashsham, J.M. Tiedje, Diverse and abundant antibiotic resistance genes in Chinese swine farms, Proc. Natl. Acad. Sci. U.S.A. 110 (2013) 3435–3440.
[7] Z.C. Zhou, W.Q. Feng, Y. Han, J. Zheng, T. Chen, Y.Y. Wei, M. Gillings, Y.G. Zhu, H. Chen, Prevalence and transmission of antibiotic resistance and microbiota between humans and water environments, Environ. Int. 121 (2018) 1155–1161.
[8] H. Hao, D.-y. Shi, D. Yang, Z.-w. Yang, Z.-g. Qiu, W.-l. Liu, Z.-q. Shen, J. Yin, H.-r. Wang, J.-w. Li, H. Wang, M. Jin, Profiling of intracellular and extracellular antibiotic resistance genes in tap water, J. Hazard Mater. 365 (2019) 340–345.
[9] M.B. Ahmed, J.L. Zhou, H.H. Ngo, W. Guo, Adsorptive removal of antibiotics from water and wastewater: progress and challenges, Sci. Total Environ. 532 (2015) 112–126.
[10] R. Xu, B. Li, E. Xiao, L.Y. Young, X. Sun, T. Kong, Y. Dong, Q. Wang, Z. Yang, L. Chen, W. Sun, Uncovering microbial responses to sharp geochemical gradients in a terrace contaminated by acid mine drainage, Environ. Pollut. Barking, Essex 261 (2020), 114226-114226.
[11] R. Xu, Z.-H. Yang, Y. Zheng, Q.-P. Wang, Y. Bai, J.-B. Liu, Y.-R. Zhang, W.-P. Xiong, Y. Lu, C.-Z. Fan, Metagenomic analysis reveals the effects of long-term antibiotic pressure on sludge anaerobic digestion and antimicrobial resistance risk, Bioresour. Technol. 282 (2019) 179–188.
[12] J. Cao, S. Sun, X. Li, Z. Yang, W. Xiong, Y. Wu, M. Jia, Y. Zhou, C. Zhou, Y. Zhang, Efficient charge transfer in aluminum-cobalt layered double hydroxide derived from Co-ZIF for enhanced catalytic degradation of tetracycline through peroxymonosulfate activation, Chem. Eng. J. 382 (2020) 122802.
[13] X.-L. Chen, L. Zhang, J.-J. Feng, W. Wang, P.-X. Yuan, D.-M. Han, A.-J. Wang, Facile solvothermal fabrication of polypyrrole sheets supported dendritic platinum-cobalt nanoclusters for highly efficient oxygen reduction and ethylene glycol oxidation, J. Colloid Interface Sci. 530 (2018) 394–402.

[14] F. Liu, W. Li, D. Wu, T. Tian, J.-F. Wu, Z.-M. Dong, G.-C. Zhao, New insight into the mechanism of peroxymonosulfate activation by nanoscaled lead-based spinel for organic matters degradation: a singlet oxygen-dominated oxidation process, J. Colloid Interface Sci. 572 (2020) 318–327.
[15] T.E. Agustina, H.M. Ang, V.K. Vareek, A review of synergistic effect of photocatalysis and ozonation on wastewater treatment, J. Photochem. Photobiol. C Photochem. Rev. 6 (2005) 264–273.
[16] F.J. Beltran, A. Aguinaco, J.F. Garcia-Araya, A.L. Oropesa, Ozone and photocatalytic processes to remove the antibiotic sulfamethoxazole from water, Water Res. 42 (2008) 3799–3808.
[17] E. Chatzisymeon, S. Foteinis, D. Mantzavinos, T. Tsoutsos, Life cycle assessment of advanced oxidation processes for olive mill wastewater treatment, J. Clean. Prod. 54 (2013) 229–234.
[18] M. Mehrjouei, S. Mueller, D. Moeller, Energy consumption of three different advanced oxidation methods for water treatment: a cost-effectiveness study, J. Clean. Prod. 65 (2014) 178–183.
[19] K. Sekiguchi, W. Morinaga, K. Sakamoto, H. Tamura, F. Yasui, M. Mehrjouei, S. Mueller, D. Moeller, Degradation of VOC gases in liquid phase by photocatalysis at the bubble interface, Appl. Catal. B Environ. 97 (2010) 190–197.
[20] C. Liu, S. Liu, L. Liu, X. Tian, L. Liu, Y. Xia, X. Liang, Y. Wang, Z. Song, Y. Zhang, R. Li, Y. Liu, F. Qi, W. Chu, D.C.W. Tsang, B. Xu, H. Wang, A. Ikhlaq, Novel carbon based Fe-Co oxides derived from Prussian blue analogues activating peroxymonosulfate: refractory drugs degradation without metal leaching, Chem. Eng. J. 379 (2020) 122274.
[21] X. Pang, Y. Guo, Y. Zhang, B. Xu, F. Qi, LaCoO3 perovskite oxide activation of peroxymonosulfate for aqueous 2-phenyl-5-sulfobenzimidazole degradation: effect of synthetic method and the reaction mechanism, Chem. Eng. J. 304 (2016) 897–907.
[22] R. Yuan, L. Hu, P. Yu, H. Wang, Z. Wang, J. Fang, Nanostructured Co3O4 grown on nickel foam: an efficient and readily recyclable 3D catalyst for heterogeneous peroxymonosulfate activation, Chemosphere 198 (2018) 204–215.
[23] K.H. Chan, W. Chu, Degradation of atrazine by cobalt-mediated activation of peroxymonosulfate: different cobalt counteranions in homogenous process and cobalt oxide catalysts in photolytic heterogeneous process, Water Res. 43 (2009) 2513–2521.
[24] T. Olmez-Hanci, I. Arslan-Alaton, Comparison of sulfate and hydroxyl radical based advanced oxidation of phenol, Chem. Eng. J. 224 (2013) 10–16.
[25] Q. Yue, Y. Yao, L. Luo, T. Hu, L. Shen, Activation of peroxymonosulfate by surfactants as the metal-free catalysts for organic contaminant removal, Environ. Sci. Pollut. Control Ser. 24 (2017) 26069–26078.
[26] J. Yu, W. Xiong, X. Li, Z. Yang, J. Cao, M. Jia, R. Xu, Y. Zhang, Functionalized MIL-53(Fe) as efficient adsorbents for removal of tetracycline antibiotics from aqueous solution, Microporous Mesoporous Mater. 290 (2019) 109642.
[27] G.P. Anipsitakis, D.D. Dionysiou, Radical generation by the interaction of transition metals with common oxidants, Environ. Sci. Technol. 38 (2004) 3705–3712.
[28] X. Li, A.I. Rykov, B. Zhang, Y. Zhangc, J. Wang, Graphene encapsulated FexCoy nanocages derived from metal-organic frameworks as efficient activators for peroxymonosulfate, Catal. Sci. Technol. 6 (2016) 7486–7494.
[29] G.R. Williams, A.I. Khan, D. O'Hare, Mechanistic and kinetic studies of guest ion intercalation into layered double hydroxides using time-resolved, in-situ X-ray power diffraction, Struct. Bond 119 (2006) 161–192.
[30] M.R. Othman, Z. Helwani, W.J.N. Fernando Martunus, Synthetic hydrotalcites from different routes and their application as catalysts and gas adsorbents: a review, Appl. Organomet. Chem. 23 (2009) 335–346.
[31] L.A. Utracki, M. Sepehr, E. Boccaleri, Synthetic, layered nanoparticles for polymeric nanocomposites WNCO, Polym. Adv. Technol. 18 (2007) 1–37.
[32] H.W. Olfs, L.O. Torres-Dorante, R. Eckelt, H. Kosslick, Comparison of different synthesis routes for Mg-Al layered double hydroxides (LDH): characterization of the structural phases and anion exchange properties, Appl. Clay Sci. 43 (2009) 459–464.
[33] A.N. Salak, J. Tedim, A.I. Kuznetsova, J.L. Ribeiro, L.G. Vieira, M.L. Zheludkevich, M.G.S. Ferreira, Comparative X-ray diffraction and infrared spectroscopy study of Zn-Al layered double hydroxides: vanadate vs nitrate, Chem. Phys. 397 (2012) 102–108.
[34] H. Zhang, B. Xia, P. Wang, Y. Wang, Z. Li, Y. Wang, L. Feng, X. Li, S. Du, From waste to waste treatment: mesoporous magnetic NiFe2O4/ZnCuCr-layered double hydroxide composite for wastewater treatment, J. Alloys Compd. 819 (2020) 153053.
[35] W.-W. Xiong, E.U. Athresh, Y.T. Ng, J. Ding, T. Wu, Q. Zhang, Growing crystalline chalcogenidoarsenates in surfactants: from zero-dimensional cluster to three-dimensional framework, J. Am. Chem. Soc. 135 (2013) 1256–1259.
[36] W.-W. Xiong, J. Miao, K. Ye, Y. Wang, B. Liu, Q. Zhang, Threading chalcogenide layers with polymer chains, Angew. Chem. Int. Ed. 54 (2015) 546–550.
[37] D.-S. Liu, Z.-J. Qiu, X. Fu, Y.-Z. Liu, P. Ding, Y.-X. Zhu, Y. Sui, Synthesis, structures and properties of three lead coordination polymers based on ethylenediaminetetraacetate ligand, J. Solid State Chem. 278 (2019) 120879.
[38] D.-S. Liu, Y. Sui, G.-M. Ye, H.-y. Wang, J.-Q. Liu, W.-T. Chen, Synthesis, structures and properties of three mercury coordination polymers based on 5-methyltetrazolate ligand, J. Solid State Chem. 263 (2018) 182–189.
[39] D.-S. Liu, Y. Sui, W.-T. Chen, P. Feng, Two new nonlinear optical and ferroelectric Zn(II) compounds based on nicotinic acid and tetrazole derivative ligands, Cryst. Growth Des. 15 (2015) 4020–4025.
[40] U.P.N. Tran, K.K.A. Le, N.T.S. Phan, Expanding applications of metal-organic frameworks: zeolite imidazolate framework ZIF-8 as an efficient heterogeneous catalyst for the knoevenagel reaction, ACS Catal. 1 (2011) 120–127.
[41] M. Zhu, D. Srinivas, S. Bhogeswararao, P. Ratnasamy, M.A. Carreon, Catalytic activity of ZIF-8 in the synthesis of styrene carbonate from CO2 and styrene oxide, Catal. Commun. 32 (2013) 36–40.
[42] Y.-H. Qin, L. Huang, D.-L. Zhang, L.-G. Sun, Mixed-node A-Cu-BTC and porous carbon based oxides derived from A-Cu-BTC as low temperature NO-CO catalyst, Inorg. Chem. Commun. 66 (2016) 64–68.
[43] Z.H. Yang, J. Cao, Y.P. Chen, X. Li, W.P. Xiong, Y.Y. Zhou, C.Y. Zhou, R. Xu, Y.R. Zhang, Mn-doped zirconium metal-organic framework as an effective adsorbent for removal of tetracycline and Cr(VI) from aqueous solution, Microporous Mesoporous Mater. 277 (2019) 277–285.
[44] Q.-G. Zhai, X. Bu, X. Zhao, D.-S. Li, P. Feng, Pore space partition in metal-organic frameworks, Acc. Chem. Res. 50 (2017) 407–417.
[45] K.-B. Wang, Q. Xun, Q. Zhang, Recent progress in metal-organic frameworks as active materials for supercapacitors, EnergyChem 2 (2020) 100025.
[46] K. Wang, R. Bi, M. Huang, B. Lv, H. Wang, C. Li, H. Wu, Q. Zhang, Porous cobalt metal-organic frameworks as active elements in battery-supercapacitor hybrid devices, Inorg. Chem. 59 (2020) 6808–6814.
[47] K.B. Wang, Q.Q. Li, Z.J. Ren, C. Li, Y. Chu, Z.K. Wang, M.D. Zhang, H. Wu, Q.C. Zhang, 2D metal-organic frameworks (MOFs) for high-performance BatCap hybrid devices, Small 16 (2020) 6.
[48] K. Wang, B. Lv, Z. Wang, H. Wu, J. Xu, Q. Zhang, Two-fold interpenetrated Mn-based metal-organic frameworks (MOFs) as battery-type electrode materials for charge storage, Dalton Trans. 49 (2020) 411–417.
[49] J. Cao, Z. Yang, W. Xiong, Y. Zhou, Y. Wu, M. Jia, S. Sun, C. Zhou, Y. Zhang, R. Zhong, Peroxymonosulfate activation of magnetic Co nanoparticles relative to an N-doped porous carbon under confinement: boosting stability and performance, Separ. Purif. Technol. 250 (2020) 117237.
[50] P. He, X.-Y. Yu, X.W. Lou, Carbon-incorporated nickel-cobalt mixed metal phosphide nanoboxes with enhanced electrocatalytic activity for oxygen evolution, Angew. Chem. Int. Ed. 56 (2017) 3897–3900.
[51] Z. Jiang, Z. Li, Z. Qin, H. Sun, X. Jiao, D. Chen, LDH nanocages synthesized with MOF templates and their high performance as supercapacitors, Nanoscale 5 (2013) 11770–11775.
[52] J. Han, J. Zhang, T. Wang, Q. Xiong, W. Wang, L. Cao, B. Dong, Zn doped FeCo layered double hydroxide nanoneedle arrays with partial amorphous phase for efficient oxygen evolution reaction, ACS Sustain. Chem. Eng. 7 (2019) 13105–13114.
[53] B. Zhang, Z. Qi, Z. Wu, Y.H. Lui, T.-H. Kim, X. Tang, L. Zhou, W. Huang, S. Hu, Defect-rich 2D material networks for advanced oxygen evolution catalysts, ACS Energy Lett. 4 (2018) 328–336.
[54] S. Yu, X. Wang, Y. Liu, Z. Chen, Y. Wu, Y. Liu, H. Pang, G. Song, J. Chen, X. Wang, Efficient removal of uranium(VI) by layered double hydroxides supported nanoscale zero-valent iron: a combined experimental and spectroscopic studies, Chem. Eng. J. 365 (2019) 51–59.
[55] X. Qiao, H. Kang, J. Wu, Y. Li, Q. Wang, X. Jia, Y. Qiao, S. Lu, X. Wu, W. Qin, A partial sulfidation approach that significantly enhance the activity of FeCo layered double hydroxide for oxygen evolution reaction, Int. J. Hydrogen Energy 44 (2019) 31987–31994.
[56] X. Xu, X. Zou, S. Wu, L. Wang, X. Niu, X. Li, J. Pan, H. Zhao, M. Lan, In situ formation of fluorescent polydopamine catalyzed by peroxidase-mimicking FeCo-LDH for pyrophosphate ion and pyrophosphatase activity detection, Anal. Chim. Acta 1053 (2019) 89–97.
[57] W. Wu, F. Lin, X. Yang, B. Wang, X. Lu, Q. Chen, F. Ye, S. Zhao, Facile synthesis of magnetic carbon nanotubes derived from ZIF-67 and application to magnetic solid-phase extraction of profens from human serum, Talanta 207 (2020) 120284.
[58] C. Gong, F. Chen, Q. Yang, K. Luo, F. Yao, S. Wang, X. Wang, J. Wu, X. Li, D. Wang, G. Zeng, Heterogeneous activation of peroxymonosulfate by Fe-Co layered doubled hydroxide for efficient catalytic degradation of Rhoadmine B, Chem. Eng. J. 321 (2017) 222–232.
[59] J. Qin, S. Wang, X. Wang, Visible-light reduction CO2 with dodecahedral zeolitic imidazolate framework ZIF-67 as an efficient co-catalyst, Appl. Catal. B Environ. 209 (2017) 476–482.
[60] J. Cao, L. Lai, B. Lai, G. Yao, X. Chen, L. Song, Degradation of tetracycline by peroxymonosulfate activated with zero-valent iron: performance, intermediates, toxicity and mechanism, Chem. Eng. J. 364 (2019) 45–56.
[61] H. Wang, Q. Gao, H. Li, B. Han, K. Xia, C. Zhou, One-pot synthesis of a novel hierarchical Co(II)-doped TiO2 nanostructure: toward highly active and durable catalyst of peroxymonosulfate activation for degradation of antibiotics and other organic pollutants, Chem. Eng. J. 368 (2019) 377–389.
[62] M. Rahm, T. Zeng, R. Hoffmann, Electronegativity seen as the ground-state average valence electron binding energy, J. Am. Chem. Soc. 141 (2019) 342–351.
[63] P. Song, Q. Song, Z. Yang, G. Zeng, H. Xu, X. Li, W. Xiong, Numerical simulation and exploration of electrocoagulation process for arsenic and antimony removal:

electric field, flow field, and mass transfer studies, J. Environ. Manag. 228 (2018) 336–345.
[64] P. Song, Z. Yang, H. Xu, J. Huang, X. Yang, F. Yue, L. Wang, Arsenic removal from contaminated drinking water by electrocoagulation using hybrid Fe-Al electrodes: response surface methodology and mechanism study, Desalination Water Treat. 57 (2016) 4548–4556.
[65] M. Ding, W. Chen, H. Xu, Z. Shen, T. Lin, K. Hu, C.H. Lu, Z. Xie, Novel alpha-Fe2O3/MXene nanocomposite as heterogeneous activator of peroxymonosulfate for the degradation of salicylic acid, J. Hazard Mater. 382 (2020) 121064.
[66] Y. Wang, S. Zhao, W. Fan, Y. Tian, X. Zhao, The synthesis of novel Co–Al2O3 nanofibrous membranes with efficient activation of peroxymonosulfate for bisphenol A degradation, Environ. Sci. J. Integr. Environ. Res.: Nano 5 (2018) 1933–1942.
[67] C. Lyu, D. He, Y. Chang, Q. Zhang, F. Wen, X. Wang, Cobalt oxyhydroxide as an efficient heterogeneous catalyst of peroxymonosulfate activation for oil-contaminated soil remediation, Sci. Total Environ. 680 (2019) 61–69.
[68] F. Chen, Q. Yang, F. Yao, S. Wang, J. Sun, H. An, K. Yi, Y. Wang, Y. Zhou, L. Wang, X. Li, D. Wang, G. Zeng, Visible-light photocatalytic degradation of multiple antibiotics by AgI nanoparticle-sensitized Bi5O7I microspheres: enhanced interfacial charge transfer based on Z-scheme heterojunctions, J. Catal. 352 (2017) 160–170.
[69] M. Jia, Z. Yang, H. Xu, P. Song, W. Xiong, J. Cao, Y. Zhang, Y. Xiang, J. Hu, C. Zhou, Y. Yang, W. Wang, Integrating N and F co-doped TiO2 nanotubes with ZIF-8 as photoelectrode for enhanced photo-electrocatalytic degradation of sulfamethazine, Chem. Eng. J. 388 (2020) 124388.